The infrared spectrum of the He–C2D2 complex

N. Moazzen-Ahmadi, A. R. W. McKellar, Berta Fernández, and David Farrelly

Citation: The Journal of Chemical Physics **142**, 084312 (2015); doi: 10.1063/1.4913492
View online: http://dx.doi.org/10.1063/1.4913492
View Table of Contents: http://scitation.aip.org/content/aip/journal/jcp/142/8?ver=pdfcov
Published by the AIP Publishing

The infrared spectrum of the He–C_2D_2 complex

N. Moazzen-Ahmadi,[1] A. R. W. McKellar,[2] Berta Fernández,[3] and David Farrelly[4]
[1]*Department of Physics and Astronomy, University of Calgary, 2500 University Drive North West, Calgary, Alberta T2N 1N4, Canada*
[2]*National Research Council of Canada, Ottawa, Ontario K1A 0R6, Canada*
[3]*Department of Physical Chemistry, and Center for Research in Biological Chemistry and Molecular Materials (CIQUS), University of Santiago de Compostela, E-15782 Santiago de Compostela, Spain*
[4]*Department of Chemistry and Biochemistry, Utah State University, Logan, Utah 84322-0300, USA*

(Received 6 January 2015; accepted 12 February 2015; published online 26 February 2015)

Spectra of the helium-acetylene complex are elusive because this weakly bound system lies close to the free rotor limit. Previously, limited assignments of He–C_2D_2 transitions in the $R(0)$ region of the ν_3 fundamental band ($\approx$2440 cm^{-1}) were published. Here, new He–C_2D_2 infrared spectra of this band are obtained using a tunable optical parametric oscillator laser source to probe a pulsed supersonic slit jet expansion from a cooled nozzle, and the analysis is extended to the weaker and more difficult $P(1)$ and $R(1)$ regions. A term value approach is used to obtain a consistent set of "experimental" energy levels. These are compared directly with calculations using two recently reported *ab initio* intermolecular potential energy surfaces, which exhibit small but significant differences. Rovibrational energies for the He–C_2H_2 complex are also calculated using both surfaces. A Coriolis model, useful for predicting spectral intensities, is used to interpret the energy level patterns, and a comparison with the isoelectronic complex He–CO is made. © *2015 AIP Publishing LLC.* [http://dx.doi.org/10.1063/1.4913492]

I. INTRODUCTION

Van der Waals complexes containing helium tend to be difficult to study spectroscopically because of their relatively weak binding and large-amplitude internal motions. For many He complexes, these challenges have long since been overcome, but helium–acetylene remains a particularly difficult case, with no published experimental spectra available until quite recently.

Detailed predictions for He–C_2H_2 based on empirical[1,2] and *ab initio* intermolecular potential surfaces were reported in 1992 by Slee *et al.*[3] Subsequently, an improved *ab initio* surface was presented by Moszynski *et al.*[4] together with predicted energy levels and spectra. Around the same time, there were also unpublished experimental results on He–C_2H_2 from the R. E. Miller laboratory (University of North Carolina) as mentioned in both Refs. 3 and 4. But it appears that detailed assignment of these infrared spectra, which were from the C_2H_2 ν_3 band region ($\approx$3300 cm^{-1}), was not possible, even with help from theory. The main problem is that this complex lies close to the free rotor limit, so that most of the intensity in the spectrum piles up in tangles of overlapping lines located near the monomer (acetylene) rotation-vibration transitions, $R(0)$, $R(1)$, $P(1)$, etc.

No further helium-acetylene spectra were reported until 2012, when we published theoretical and experimental results on He–C_2D_2 including detailed rotational assignments.[5] At that time, our results were limited to the $R(0)$ part of the spectrum, namely, transitions in the $j = 1 \leftarrow 0$ region of the C_2D_2 ν_3 band ($\approx$2440 cm^{-1}), where j represents the (relatively unhindered) rotation of C_2D_2 within the complex. Reasons for this limitation are explained below. With the help of improved spectra, it is now possible to extend our analysis to the $j = 0 \leftarrow 1$ and $2 \leftarrow 1$ regions as reported in the present paper, thus obtaining a much more complete picture of He–C_2D_2 rotational energy levels. In the remainder of the paper, quantum number v will refer to ν_3 of C_2D_2. Other rare gas–acetylene complexes whose spectra have been studied are those containing Ne,[6,7] Ar,[8–17] and Kr.[18,19]

Very recently, pure rotational Raman-type transitions with $\Delta J = 2$ have been measured in He–C_2H_2 by observing rotational wave packets in the time domain following impulsive alignment by a femtosecond laser pulse.[20,21] In these papers, comparisons were also made between the observed transitions and rovibrational energies computed using a new *ab initio* potential energy surface. In the present paper, we report our experimental infrared spectra of He–C_2D_2 in conjunction with calculations based on the helium–acetylene potential energy surface of Fernández *et al.*[22] In addition, we make comparisons with the new surface of Galinis *et al.*[21] and find that our He–C_2D_2 spectra are accurate enough to discriminate between the two surfaces.

II. THEORETICAL *AB INITIO* ENERGY LEVELS

The general characteristics and appropriate labelling scheme for He–C_2D_2 rotational levels were discussed in Ref. 5. Here, we summarize that discussion, and extend the results to levels with $j = 2$. Use of the approximate quantum number j is appropriate because the barrier to free internal rotation of acetylene within the complex is small. For $j = 0$, there is a single "stack" of rotational levels with $J = 0$, 1, 2, etc., which have even parity, denoted e.[23] For $j = 1$, there are three stacks. One is labelled σ, starts with $J = 0$, has e parity, and corresponds to the first excited bending state in a normal

semi-rigid T-shaped molecule, or to the σ-bending overtone in a normal linear molecule. The other two stacks, labelled π, start with $J = 1$ and correspond to asymmetric rotor $K = 1$ levels in the T-shaped limit or to the first excited π-bending levels in the linear limit. One π stack has e parity and the other f parity. The $j = 1$ stacks with e parity (σ and π) become increasingly mixed for $J \geq 1$ by a Coriolis interaction, so their labelling as σ or π can become somewhat arbitrary, especially when close to the free rotation limit. As pointed out previously,[3,5] the distinction between the 1σ stack being located above or below the 1π stack corresponds approximately to a T-shaped or linear structure, respectively, for the complex. For $j = 2$, there are five stacks: a single σ stack with e parity, a pair (e and f) of π stacks, and a pair (e and f) of δ stacks which start with $J = 2$. All $j = 2$ levels are affected by Coriolis mixing, except for the unique levels $J = 0$ of σe and $J = 1$ of πf.

The recent new potential surface for helium–acetylene, called IPESA here, obtained at the CCSD(T) level by Fernández *et al.*[22] is used in our calculations. It is an extended version of the earlier Fernández and Munteanu[24] surface, with a global energy minimum at −24.21 cm^{-1} for the linear configuration with intermolecular distance $R = 4.345$ Å, and a saddle point at the T-shaped geometry ($E = -16.7$ cm^{-1}, $R = 3.82$ Å). Rotational levels calculated using the earlier potential and the BOUND program[25] were reported for $j = 0$ and 1 in Ref. 5. Slightly different levels based on the newer potential are given here in Fig. 1 and Table I, and they are augmented by a number of calculated $j = 2$ levels. Levels are labelled by j (=0, 1, or 2), by K (=σ, π, or δ), by the parity p (=e or f), and by the total angular momentum, J. Also included for completeness is the end-over-end rotational quantum number L, which is discussed below in Sec. VII B. Energies are expressed relative to the lowest 0 σe level with $J = 0$, which is calculated[22] to lie 7.2360 cm^{-1} below the dissociation limit. Note that the dissociation threshold for odd-j levels (that is, for *para*-C_2D_2) actually lies about 1.7 cm^{-1} (=2B for C_2D_2) higher than that for even-j levels (*ortho*-C_2D_2), as shown in Fig. 1. For comparison, Table I also shows the levels calculated using the recent potential energy surface reported in Refs. 20 and 21, called IPESB here.

III. THE CORIOLIS MODEL FOR ROTATIONAL ENERGIES

We showed in Ref. 5 that a simple Coriolis model[26,27] was useful for representing the $j = 1$ energy levels of He–C_2D_2 as well as the observed transition intensities in the $j = 1 \leftarrow 0$ subband. Here, we extend the model to include the $j = 2$ levels, with the notation changed slightly to adapt better to $j = 2$.

The $j = 0$ σe and $j = 1$ πf stacks are not affected by Coriolis interactions, since in each case there are no other levels with the same values of J, j, and e/f symmetry. Thus, they have simple linear molecule rotational energies given by

$$E(0\ \sigma e) = B(0)J(J+1) - D(0)[J(J+1)]^2,$$
$$E(1\ \pi f) = E_v(1\pi) + B(1\pi)J(J+1) - D(1\pi)[J(J+1)]^2.$$

The $j = 1$ σe and 1 πe stacks are coupled by a Coriolis interaction. Their energies are given by diagonalizing a 2×2 matrix with diagonal elements

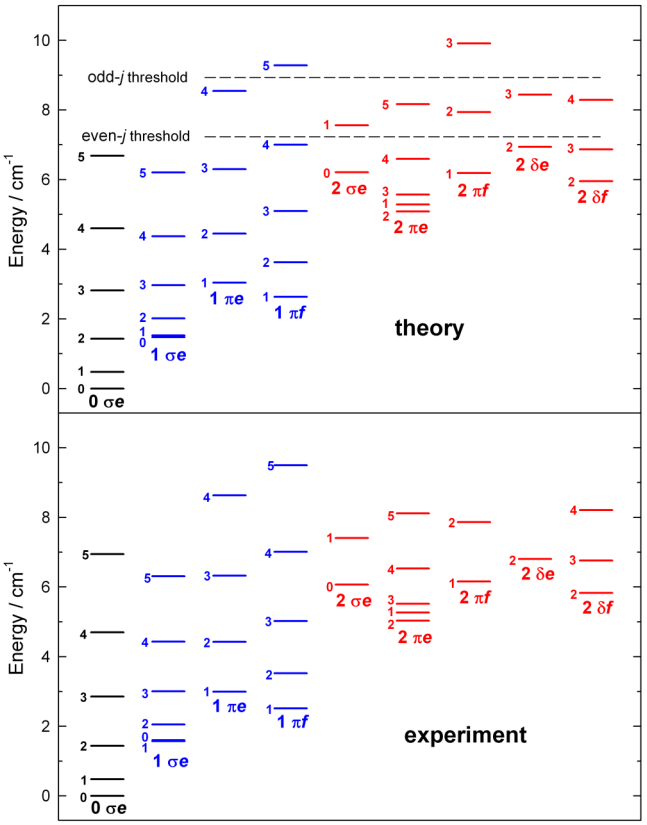

FIG. 1. Theoretical and "experimental" energy levels for He–C_2D_2 (Table I). The experimental data are for the v = 1 state of C_2D_2. Each stack is labelled by j, K (=σ, π, or δ), and p (=e or f), and each level is labelled on the left by J. Dashed lines show the theoretical thresholds (dissociation limits) for even and odd j-values.

$$E(1\ \sigma e) = E_v(1\sigma) + B(1\sigma)J(J+1) - D(1\sigma)[J(J+1)]^2 \text{ and}$$
$$E(1\ \pi e) = E_v(1\pi) + B(1\pi)J(J+1) - D(1\pi)[J(J+1)]^2,$$

and off-diagonal elements given by $[\beta(1)J(J+1)]^{1/2}$, where β characterizes the strength of the Coriolis interaction. The stack origins $E_v(1\sigma)$ and $E_v(1\pi)$ are related to the former[5] parameters E_{vr} and α as follows: $E_{vr} = (E_v(1\sigma) + E_v(1\pi))/2$ and $\alpha = (E_v(1\pi) - E_v(1\sigma))/2$.

The $j = 2$ levels are represented in an analogous manner, with diagonal energies given by

$$E(2\ \sigma e) = E_v(2\sigma) + B(2\sigma)J(J+1),$$
$$E(2\ \pi e/f) = E_v(2\pi) + B(2\pi)J(J+1),$$
$$E(2\ \delta e/f) = E_v(2\delta) + B(2\delta)J(J+1).$$

The e levels are obtained by diagonalizing a 3×3 matrix with off-diagonal element $[\beta(2)J(J+1)]^{1/2}$ connecting the (2 σe) and (2 πe) levels, and off-diagonal element $[\gamma(2)(J(J+1)-2)]^{1/2}$ connecting the (2 πe) and (2 δe) levels. The f levels are obtained by diagonalizing a 2×2 matrix with off-diagonal element $[\gamma(2)(J(J+1)-2)]^{1/2}$ connecting the (2 πf) and (2 δf) levels. We omit centrifugal distortion terms (D) for $j = 2$ in order to limit the number of free parameters in consideration of the limited number of observed or calculated $j = 2$ levels to be fitted.

The first columns of Table II show the results of fitting this model to the theoretical levels of Table I. For $j = 0$ and 1,

TABLE I. Theoretical and "experimental" rotational energy levels of He–C_2D_2 (units of cm^{-1}).[a]

				v = 0			v = 1
j	Kp	J	L	IPESA[b]	IPESB[c]	Experiment	Experiment[d]
0	σ*e*	0	0	0.0	0.0	0.0	0.0
0	σ*e*	1	1	0.4789(−44)	0.4802(−44)	0.4843(0)	0.4821(0)
0	σ*e*	2	2	1.4257(−76)	1.4291(−76)	1.4456(0)	1.4382(0)
0	σ*e*	3	3	2.8146(−25)	2.8194(−22)	2.8699(0)	2.8520(0)
0	σ*e*	4	4	4.5947(+95)	4.5969(+91)	4.7355(0)	4.6990(0)
0	σ*e*	5	5	6.6681(−35)	6.6627(−34)	7.0139(0)	6.9465(0)
1	σ*e*	0	1	1.4744(+26)	1.3789(+30)	1.5535(+19)	1.5982(+18)
1	σ*e*	1	0	1.5243(−143)	1.4737(−115)	1.5557(−43)	1.5747(−128)
1	σ*e*	2	1	2.0133(−131)	1.9799(−112)	2.0414(+6)	2.0516(−105)
1	σ*e*	3	2	2.9657(−15)	2.9445(−12)	2.9962(+13)	3.0069(−18)
1	σ*e*	4	3	4.3687(+102)	4.3605(+88)	4.4166(−2)	4.4312(+69)
1	σ*e*	5	4	6.1940(+39)	6.2037(+31)	6.2990(−1)	6.3101(+39)
1	π*e*	1	2	3.0377(+159)	3.0914(+130)	3.0092(+19)	2.9937(+112)
1	π*e*	2	3	4.4441(+333)	4.4960(+305)	4.4445(−15)	4.4220(+178)
1	π*e*	3	4	6.2913(+259)	6.3550(+250)		6.3261(+264)
1	π*e*	4	5	8.5248(−391)	8.6091(−356)		8.6365(−328)
1	π*f*	1	1	2.6331(−148)	2.7277(−145)	2.5604(+6)	2.5141(−111)
1	π*f*	2	2	3.6263(−131)	3.7281(−128)	3.5650(−4)	3.5221(−27)
1	π*f*	3	3	5.0912(−56)	5.2044(−57)	5.0566(+1)	5.0227(+12)
1	π*f*	4	4	6.9916(+73)	7.1216(+62)	7.0122(0)	7.0109(−17)
1	π*f*	5	5	9.2565(+25)	9.4136(+30)		9.4980(+41)
2	σ*e*	0	2	6.2069(+319)	6.2674(+289)		6.0708(+179)
2	σ*e*	1	3	7.5174(−375)	7.5668(−350)		7.4032(−258)
2	π*e*	1	1	5.2859(+81)	5.2794(+140)		5.2658(+215)
2	π*e*	2	0	5.0890(−236)	5.1090(−212)		5.0311(−147)
2	π*e*	3	1	5.5709(−340)	5.6055(−370)		5.5168(−311)
2	π*e*	4	2	6.5908(−225)	6.6538(−268)		6.5325(−320)
2	π*e*	5	3	8.1557(+350)	8.2664(+386)		8.1133(+358)
2	π*f*	1	2	6.1881(+234)	6.1451(+282)		6.1589(+200)
2	π*f*	2	3	7.9827(+517)	7.9917(+184)		7.8655(−126)
2	π*f*	3	4	9.9037(−408)	9.9870(−227)		
2	δ*e*	2	2	6.9390(+9)	7.0708(+83)		6.8052(+27)
2	δ*e*	3	3	8.4340(+40)	8.5770(+11)		
2	δ*f*	2	1	5.9526(−56)	6.0158(+7)		5.8308(+152)
2	δ*f*	3	2	6.8682(+72)	6.9315(+76)		6.7625(+119)
2	δ*f*	4	3	8.2873(+17)	8.3593(−30)		8.2063(−89)

[a]Quantities in parentheses are residuals (observed minus calculated) in units of 0.0001 cm^{-1}, with calculations based on Coriolis model parameters (Table II). Experimental $j = 0$ levels are defined by $B(0)$ and $D(0)$ so these residuals are zero.
[b]Calculated from the *ab initio* potential surface IPESA.[22]
[c]Calculated from the *ab initio* potential surface IPESB.[20,21]
[d]Relative to the estimated band origin, 2439.2800 cm^{-1} (see text).

the parameters are slightly different than reported previously[5] because there are now separate D-values for the (1σ) and (1π) states. For $j = 2$, we obtain an acceptable, but not perfect, fit, whose quality can be judged by the residuals given in parentheses in Table I. The values of the resulting parameters appear to be reasonable. Note in particular that the fitted B-values for $j = 2$ are similar to those for $j = 1$, and that the Coriolis parameter $\beta(2)^{1/2}$ is larger than $\beta(1)^{1/2}$ by a factor of 1.72 (for IPESA). This is close to the factor of $3^{1/2} = 1.73$ which is predicted by the expression $\beta \approx 2Bj^*(j^* + 1)$, where j^* is an effective value which approaches j in the free rotor limit.[26]

IV. THE SPECTRUM OF He–C_2D_2

The spectra were recorded using a previously described pulsed supersonic slit jet apparatus at the University of Calgary,[28] with a Lockheed Martin Aculight Argos optical parametric oscillator (OPO) as the laser probe. In contrast to our previous He–C_2D_2 work,[5] the jet nozzle was cooled to about −75 C. Combined with an even more dilute expansion gas mixture (≈0.04% C_2D_2 in helium), the cold nozzle helped to greatly boost the strength of the He–C_2D_2 transitions relative to those of the acetylene dimer, $(C_2D_2)_2$.[29,30] Wavenumber calibration utilized signals from a fixed etalon and from a reference

TABLE II. Coriolis model fits for rotational levels of He–C_2D_2.[a]

	v = 0			v = 1
	IPESA[b]	IPESB[b]	Experiment	Experiment
$E_v(0)$	0.0	0.0	0.0	2439.280 0
$B(0)$	0.243 01	0.243 76	0.242 73	0.241 74
$D(0)$	0.000 69	0.000 72	0.000 30	0.000 34
$E_v(1\sigma)$	1.471 8	1.375 9	1.551 6	1.596 4[c]
$E_v(1\pi)$	2.146 1	2.237 1	2.053 5	2.025 0[c]
$B(1\sigma)$	0.220 0	0.222 5	0.227 8	0.224 2
$B(1\pi)$	0.251 9	0.253 5	0.253 7	0.250 2
$\beta(1)^{1/2}$	0.455 4	0.453 4	0.473 0	0.463 0
$D(1\sigma)$	−0.000 16	−0.000 14	−0.000 08	0.000 00
$D(1\pi)$	0.000 50	0.000 48	0.000 29	0.000 04
$E_v(2\sigma)$	6.175 0	6.238 5		6.052 9[c]
$E_v(2\pi)$	5.677 4	5.623 0		5.656 2[c]
$E_v(2\delta)$	5.295 4	5.420 2		5.044 7[c]
$B(2\sigma)$	0.246 5	0.255 9		0.240 7
$B(2\pi)$	0.243 7	0.247 0		0.241 3
$B(2\delta)$	0.242 4	0.243 9		0.257 5
$\beta(2)^{1/2}$	0.785 2	0.795 1		0.759 6
$\gamma(2)^{1/2}$	0.683 8	0.687 9		0.706 1

[a]Parameters are in units of cm^{-1}. Uncertainties are not given because the number of fitted levels (12-15) is not much larger than the number (7-8) of parameters.
[b]Fitted to the theoretical levels of Table I, based on potential surfaces IPESA[22] and IPESB.[20,21]
[c]Relative to the estimated He–C_2D_2 band origin, 2439.2800 cm^{-1}.

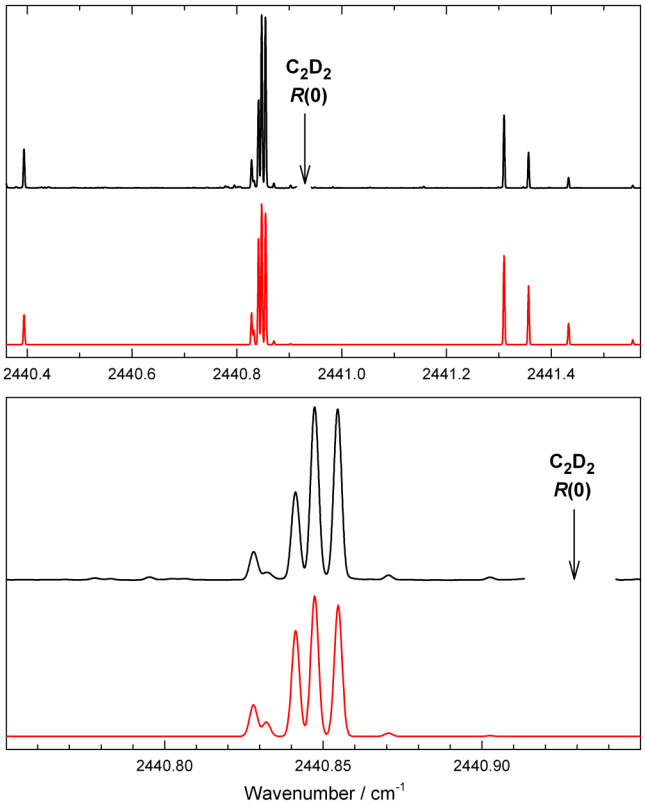

FIG. 2. Observed (upper traces) and simulated (lower traces) spectra of the $j = 1 \leftarrow 0$ subband of He–C_2D_2. The simulation is based on line positions given by experimental term values (Table I) and the intensities given by the Coriolis model (Table II) for a temperature of 1.5 K. A gap occurs in the observed spectrum around the strong C_2D_2 monomer $R(0)$ line as marked.

gas cell containing room temperature N_2O.[31] The PGOPHER computer package was used for spectral simulation.[32]

A. The $j = 1 \leftarrow 0$ subband

The strongest feature in the He–C_2D_2 spectrum is the $j = 1 \leftarrow 0$ subband, which we reported previously.[5] The present improved spectrum in this region is shown in Fig. 2, and the assigned transitions are listed in Table III. These assignments are the same as given previously, with one minor change ($P(3)$ transition, 2440.8321 cm^{-1}) and one addition ($R(1)$ transition, 2443.2177 cm^{-1}). There is a small systematic wavenumber shift (<0.002 cm^{-1}) due to improved (we hope!) calibration. As well, the relative intensities in the new spectrum are different because the effective rotational temperature is now around 1.5 K, as compared to 2.5 K previously.

B. The $j = 0 \leftarrow 1$ subband

In the low temperature jet environment, He–C_2D_2 subbands ($j = 0 \leftarrow 1$ and $2 \leftarrow 1$) originating from $j = 1$ levels tend to be weaker than the $1 \leftarrow 0$ subband due to a nuclear spin weight disadvantage, since the 2:1 spin statistics of C_2D_2 favor subbands with even values of j''. Finally, the $j = 0 \leftarrow 1$ subband occurs in a region with strong absorption from the acetylene dimer.[29,30] These are the reasons why we were not able previously to analyse $j = 0 \leftarrow 1$ transitions.

To a first approximation, we expect the $j = 0 \leftarrow 1$ subband, shown in Fig. 3, to be a mirror image of $j = 1 \leftarrow 0$. But this turns out to be only partly true. There is a single dominant He–C_2D_2 feature at 2437.72 cm^{-1} in the new $j = 0 \leftarrow 1$ spectrum which is the analog of the three strong $j = 1 \leftarrow 0$ lines at 2440.84–2440.86 cm^{-1}. Evidently, these three $j = 1 \leftarrow 0$ lines have merged into the single unresolved $j = 0 \leftarrow 1$ line. The mirror image resemblance is better for the $j = 0 \leftarrow 1$ transitions around 2437.0–2437.2 cm^{-1} which are the analog of the characteristic Q-branch series at 2441.3–2441.5 cm^{-1}. But they are much weaker, and one of them (2437.15 cm^{-1}) unfortunately falls right on top of a C_2D_2 dimer line. Some assignments in the $j = 0 \leftarrow 1$ subband were tricky, but we eventually came up with a satisfactory scheme as given in Table III, using criteria such as combination differences, consistency with the $j = 1 \leftarrow 0$ and $2 \leftarrow 1$ subbands, and relative intensities as calculated using the Coriolis model. Note that Table III is organized so that analogous (mirror image) transitions in the two subbands ($j = 1 \leftarrow 0$ and $0 \leftarrow 1$) appear on the same row.

C. The $j = 2 \leftarrow 1$ subband

The region of the $j = 2 \leftarrow 1$ subband is shown in Fig. 4. There is a very strong line at 2442.755 cm^{-1}, another seven or eight medium strength features, and a few more weak lines. The lines marked with asterisks in Fig. 4 belong to the $j = 1 \leftarrow 0$ subband (Table III). As the free rotor limit is approached, the spectral intensity distribution obviously must collapse to that of a free rotor. In other words, it becomes more and more like that of the monomer itself. Hence, most of the intensity in the $j = 2 \leftarrow 1$ subband occurs close to the monomer $R(1)$

TABLE III. Observed line positions and rotational line assignments for the $j = 1 \leftarrow 0$ and $0 \leftarrow 1$ subbands of He–C_2D_2 (values in cm^{-1}).[a]

j	Kp	J	L	j	Kp	J	L	$j = 1 \leftarrow 0$	$j = 0 \leftarrow 1$
1	πf	1	1	0	σe	1	1	2441.3098 (0)	2437.2021 (+3)
1	πf	2	2	0	σe	2	2	2441.3565 (0)	2437.1534 (+1)
1	πf	3	3	0	σe	3	3	2441.4328 (0)	2437.0754 (0)
1	πf	4	4	0	σe	4	4	2441.5554 (0)	2436.9668 (0)
1	πf	5	5	0	σe	5	5	2441.7641 (0)	
1	πe	1	2	0	σe	2	2	2440.8281 (+1)	2437.7084 (−6)
1	πe	2	3	0	σe	3	3	2440.8321 (0)	2437.6875 (0)
1	πe	3	4	0	σe	4	4	2440.8706 (0)	
1	πe	4	5	0	σe	5	5	2440.9026 (0)	
1	σe	1	0	0	σe	0	0	2440.8548 (+1)	2437.7213 (−30)
1	σe	2	1	0	σe	1	1	2440.8473 (0)	2437.7213 (+5)
1	σe	3	2	0	σe	2	2	2440.8413 (0)	2437.7213 (−7)
1	σe	4	3	0	σe	3	3	2440.8413 (0)	2437.7154 (0)
1	σe	5	4	0	σe	4	4	2440.8546 (0)	2437.6800 (0)
1	σe	0	1	0	σe	1	1	2440.3939 (0)	2438.2086 (−1)
1	σe	1	0	0	σe	2	2	2439.4090 (−1)	2439.1644 (+18)
1	σe	2	1	0	σe	3	3		2440.0898 (−8)
1	σe	3	2	0	σe	4 4		2440.9830 (+2)	
1	πe	1	2	0	σe	0	0	2442.2736 (−1)	2436.2730 (+22)
1	πe	2	3	0	σe	1	1	2443.2177 (0)	

[a]"Mirror-image" transitions of the $j = 1 \leftarrow 0$ and $0 \leftarrow 1$ subbands are on the same row. For the $j = 1 \leftarrow 0$ subband, the first set of quantum numbers (j Kp J L) refers to the upper state (v = 1) and the second set to the lower state (v = 0). For the $j = 0 \leftarrow 1$ subband, the first set of quantum numbers refers to the lower state (v = 0) and the second set to the upper state (v = 1). Quantities in parentheses are residuals (observed minus calculated) in units of 0.0001 cm^{-1}, where the calculated positions are given by the "experimental" energy levels of Table I.

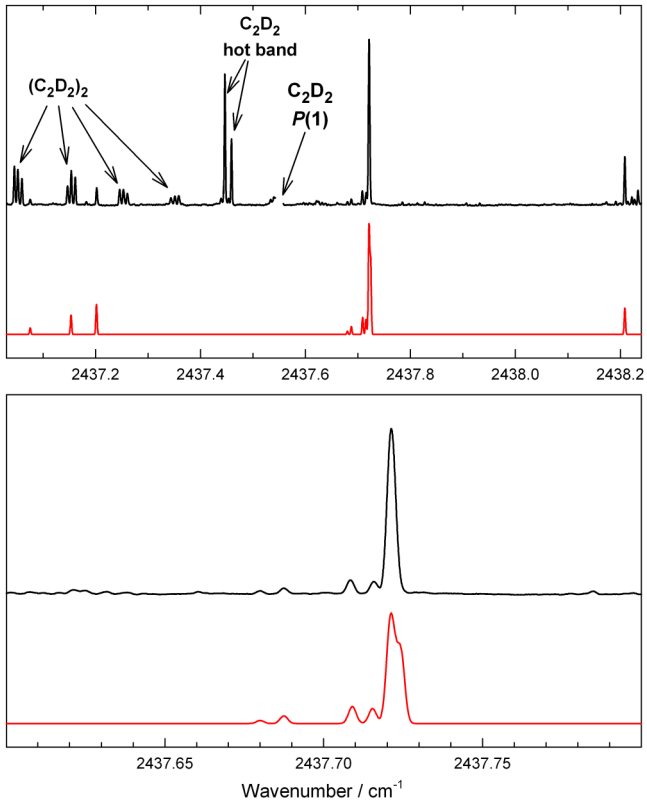

FIG. 3. Observed (upper traces) and simulated (lower traces) spectra of the $j = 0 \leftarrow 1$ subband of He–C_2D_2. The simulation is based on line positions given by experimental term values (Table I) and the intensities given by the Coriolis model (Table II) for a temperature of 1.5 K. A gap occurs in the observed spectrum around the strong C_2D_2 monomer $P(1)$ line as marked.

transition, just as most of the intensity in the $j = 1 \leftarrow 0$ and $0 \leftarrow 1$ subbands occurs close to the monomer $R(0)$ and $P(1)$ transitions.

The rotational assignment of this subband was challenging since many of the transitions lie close to each other and since we did not have a spectroscopic model which could reliably predict energies with sufficient accuracy. We were guided by the *ab initio* theoretical levels discussed in Sec. II, by the need for consistency with the $j = 0 \leftarrow 1$ subband, which shares a common lower state, and by the predictions of the Coriolis model, particularly in terms of transition intensities. Spectra recorded with different effective rotational temperatures also provided clues about the relative energies of the lower state levels. The resulting assignments are shown in Table IV. Note that the 2442.755 cm^{-1} line is assigned as a blend of two transitions, helping to explain its dominant strength. In the simulated spectra (see below), these are the two strongest transitions in the $j = 2 \leftarrow 1$ subband.

V. EXPERIMENTAL TERM VALUE AND CORIOLIS MODEL FITS

Previously, we used the Coriolis model to directly fit and simulate the $j = 1 \leftarrow 0$ subband.[5] Here, we adopt a slightly different approach in which the spectrum is first analysed in terms of "experimental" energy levels. The resulting term values (level energies) can then be directly compared with theory, as well as fitted in terms of the Coriolis (or other) model. The procedure is somewhat similar to that used for the spectra of the closely related He–CO complex.[33–35] For He–CO, it was actually possible to obtain *all* bound state energies without further assumptions. This was enabled by the availability of both microwave and infrared data, and by the fact that the infrared spectra were obtained at a "high" (47 K) temperature so that all lower state rotational levels were well populated. In the present case it is not possible to determine all levels directly, so we make a simplifying assumption, namely, that the energies for $j = 0$ can be represented with sufficient accuracy by two parameters, using the expression $BJ(J + 1) - D[J(J + 1)]^2$ (with different B- and D-values for the v = 0 and 1 states, of course). This assumption is reasonable on the basis of the *ab initio* $j = 0$ levels in Table I.

We then "fit" the observed spectra (Tables III and IV) in terms of experimental energy levels, and obtained the values given in the last two columns of Table I, as well as the residuals (observed minus calculated line positions) given in parentheses in Tables III and IV. Many levels are determined by only one transition, and such transitions fit perfectly, with zero residual. Other levels are involved in more than one transition, and may have small residuals corresponding to combination differences which do not match perfectly. Such discrepancies are due to experimental uncertainties, and more specifically to the fact that some observed lines are actually blends of two or more underlying transitions.

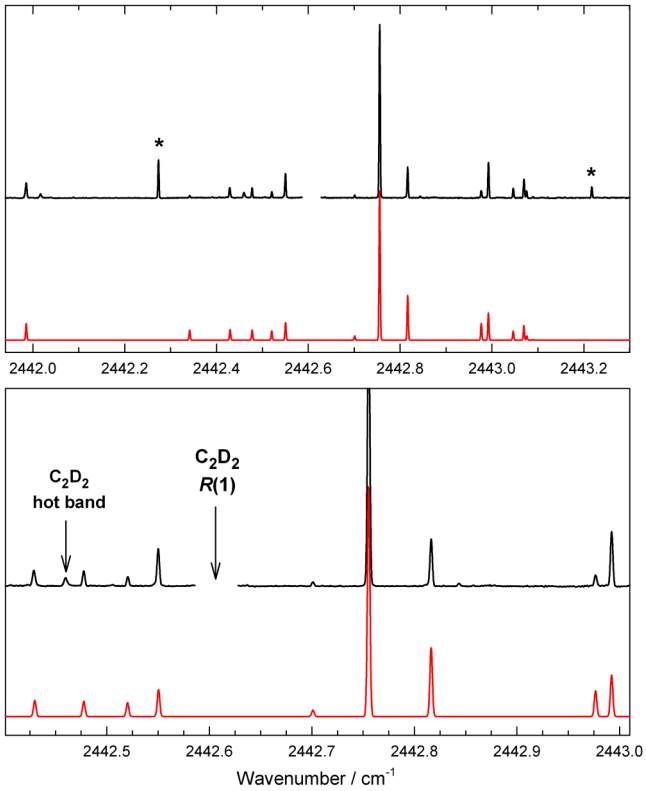

FIG. 4. Observed (upper traces) and simulated (lower traces) spectra of the $j = 2 \leftarrow 1$ subband of He–C_2D_2. The simulation is based on line positions given by experimental term values (Table I) and the intensities given by the Coriolis model (Table II) for a temperature of 1.5 K. Lines marked with an asterisk belong to the $j = 1 \leftarrow 0$ subband (see Table III). A gap occurs in the observed spectrum around the strong C_2D_2 monomer $R(1)$ line as marked.

TABLE IV. Observed line positions and rotational assignments for the $j = 2 \leftarrow 1$ subband of He–C_2D_2 (values in cm^{-1}).[a]

j	Kp	J	L	j	Kp	J	L	$j = 2 \leftarrow 1$
2	πf	1	2	1	πf	2	2	2441.8736 (−3)
2	πe	1	1	1	πf	1	1	2441.9854 (−1)
2	σe	0	2	1	πe	1	2	2442.3416 (0)
2	πf	1	2	1	πe	1	2	2442.4288 (−9)
2	δf	3	2	1	πf	2	2	2442.4775 (−1)
2	δe	2	2	1	πf	2	2	2442.5205 (+3)
2	δf	2	1	1	πf	1	1	2442.5501 (−3)
2	πf	2	3	1	πe	2	3	2442.7010 (0)
2	πe	2	0	1	σe	1	0	2442.7554 (0)
2	πe	3	1	1	σe	2	1	2442.7554 (0)
2	πe	4	2	1	σe	3	2	2442.8163 (0)
2	πe	5	3	1	σe	4	3	2442.9767 (0)
2	πe	1	1	1	σe	0	1	2442.9924 (+1)
2	δf	3	2	1	σe	3	2	2443.0464 (+1)
2	δf	2	1	1	σe	2	1	2443.0697 (+3)
2	δf	4	3	1	σe	4	3	2443.0697 (0)
2	δe	2	2	1	πe	1	2	2443.0753 (−7)
2	δe	2	2	1	σe	3	2	2443.0894 (+4)
2	πf	1	2	1	σe	1	0	2443.8844 (+12)
2	σe	1	3	1	πf	1	1	2444.1228 (0)

[a]Quantities in parentheses are residuals (observed minus calculated) in units of 0.0001 cm^{-1}, where the calculated positions are given by the "experimental" energy levels of Table I.

The He–C_2D_2 band origin cannot be directly determined from experiment because $\Delta j = 0$ infrared transitions are forbidden, but we estimate its value to be 2439.280 cm^{-1}. This represents a small vibrational blue shift of +0.036 cm^{-1} relative to the C_2D_2 monomer band origin.[36] To facilitate comparison of v = 0 and 1 levels, this band origin has been subtracted from the experimental v = 1 term values in Table I.

By fitting the experimental term values using the Coriolis model, we obtain the parameters given in the last two columns of Table II. The quality of the fits is only moderate, as can be judged from the residuals given in parentheses in Table I. The theoretical v = 0 and experimental v = 1 residuals are roughly similar in magnitude, while the experimental v = 0 residuals for $j = 1$ are smaller because fewer levels were fitted to the same number of parameters in the latter case. Considerably better fits could be obtained by including more parameters in the Coriolis model, for example, a centrifugal distortion correction to β. But this was avoided because the number of parameters then becomes perilously close to the number of fitted levels, impairing their significance and predictive value.

The line positions in the simulated (lower) traces of Figs. 2–4 are based on the fitted experimental term values, so they naturally agree almost perfectly with the experimental spectra. But the simulated intensities come from calculations using the Coriolis model parameters (Table II) and the linear molecule option of PGOPHER[32] as described previously,[5] with an assumed temperature of 1.5 K. Tests showed that these relative intensities are not very sensitive to the exact values of the Coriolis parameters. But they are quite sensitive to temperature, and over the range of 1.5–2.5 K the simulations remain consistent with experiment. Overall, the simulations explain the observed spectra very well in terms of a set of experimental rotational levels which are self-consistent and compatible with theory. This does not guarantee that all the assignments are correct, but it is probably the best that can be accomplished at present.

VI. COMPARISON OF IPESA AND IPESB

As noted, Galinis *et al.*[20,21] recently reported spectra of He–C_2H_2 obtained using rotational wave packet spectroscopy (RWPS) and a new intermolecular potential energy surface (which we label IPESB) which was used to help interpret the spectra. They noted impressive agreement between experiment and theory, and also claimed[20,21] that their potential (IPESB) is superior to IPESA, based on the implication that the RWPS results are accurate enough to discriminate between slightly different predicted equilibrium structures. To investigate this comparison further, we have calculated rovibrational levels for He–C_2D_2 (Table I) and He–C_2H_2 (Table V) using both surfaces. The same IPES should of course be capable of describing both isotopologues more or less equally well.

The RWPS results for He–C_2H_2 are compared with theory in Table VI. The root mean square (rms) deviations between theory and experiment are about 0.035 cm^{-1} for IPESA and 0.018 cm^{-1} for IPESB, as compared to the estimated[20,21] experimental uncertainty of 0.03 cm^{-1}. However, the situation is different for the infrared results on He–C_2D_2: up to $J = 4$ in

TABLE V. Calculated rotational energy levels of He–C_2H_2 (values in cm^{-1}).[a]

j	Kp	J	L	IPESA	IPESB
0	σe	0	0	0.0	0.0
0	σe	1	1	0.4863	0.4890
0	σe	2	2	1.4499	1.4579
0	σe	3	3	2.8709	2.8870
0	σe	4	4	4.7146	4.7420
1	σe	0	1	2.1257	2.0211
1	σe	1	0	2.1685	2.1113
1	σe	2	1	2.6613	2.6220
1	σe	3	2	3.6237	3.5975
1	σe	4	3	5.0423	5.0309
1	πe	1	2	3.6743	3.7204
1	πe	2	3	5.0930	5.1382
1	πe	3	4	6.9543	7.0132
1	πe	4	5	9.2040	9.2887
1	πf	1	1	3.2591	3.3483
1	πf	2	2	4.2613	4.3585
1	πf	3	3	5.7396	5.8495
1	πf	4	4	7.6567	7.7854

[a]All computed values obtained using the BOUND program. Relative to ground state energies of −7.1272 cm^{-1} (IPESA)[22] and −7.417 cm^{-1} (IPESB).[20,21]

the $j \leq 1$ stacks, the rms deviations are about 0.054 cm^{-1} for IPESA and 0.105 cm^{-1} for IPESB (see Table I). Thus, we see that IPESA is overall closer to experiment than IPESB, being almost as good for the He–C_2H_2 RWPS data (considering the experimental uncertainty) and better for the more precise and extensive He–C_2D_2 infrared data.

As discussed below, the Coriolis model results indicate that, experimentally, the He–C_2D_2 complex lies closer to the isotropic (free-rotor) limit than predicted by IPESA. However, a comparison of ground state probability densities, shown here in Fig. 5, reveals that IPESB lies significantly further from the free-rotor limit than does IPESA. In the free-rotor limit, the probability density would be structureless in the angle; that is, probability density would be uniform as a function of angle θ, although not as a function of R. As the anisotropy of the IPES increases, the probability density map (corresponding to the computed wave function using that IPES) would show marked differences (peaks and valleys) as a function of θ. Figure 5 is a difference map which, by comparing computed probability densities using IPESA and IPESB, displays the anisotropy of IPESA compared to that of IPESB. The enhanced

TABLE VI. Experimental and calculated line positions in the RWPS spectrum of He–C_2H_2 (values in cm^{-1}).

j	Kp	J	L	J	Kp	J	L	Experiment[a]	IPESA[b]	IPESB[a]
0	σe	2	2	0	σe	0	0	1.43	1.450	1.458
0	σe	3	3	0	σe	1	1	2.41	2.385	2.398
1	σe	2	1	1	σe	0	1	0.58	0.536	0.601
1	σe	3	2	1	σe	1	0	1.51	1.455	1.486
1	σe	4	3	1	σe	2	1	2.41	2.381	2.409
1	πf	3	3	1	πf	1	1	2.50	2.481	2.501

[a]References 20 and 21.
[b]Reference 22.

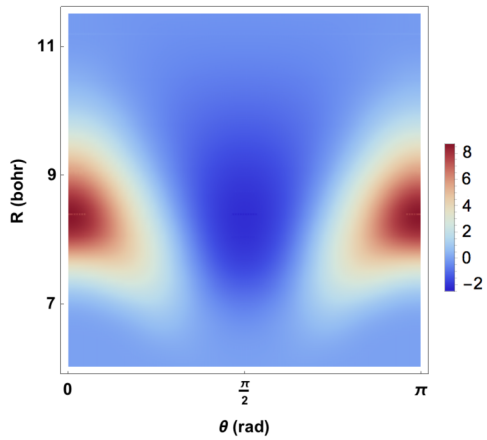

FIG. 5. Probability density difference map (d) corresponding to the ground state wave functions obtained using IPESA (ψ^A) and IPES-B (ψ^B) for He - C_2D_2; $d = 100 \times (|\psi^B|^2 - |\psi^A|^2)/|\psi^B_{max}|^2$, where ψ^B_{max} is the maximum value of ψ^B. R and θ are Jacobi coordinates.

density observed for IPESB at $\theta = 0$ and π indicates clearly that IPESB is more anisotropic than IPESA. In other words, IPESB lies noticeably further from the free-rotor (isotropic) limit than does IPESA. This is the opposite of experimental observations and is why we conclude that IPESB is inferior to IPESA in this respect.

We note that the present infrared results are about 10 times more accurate than the RWPS results[20,21] (of course, the RWPS technique may be capable of higher accuracy in the future). Furthermore, the assigned RWPS transitions all occur *within* a given j-stack, which means they depend strongly on the intermolecular distance, but are relatively insensitive to anisotropy in the potential surface. In contrast, infrared transitions *between* j-stacks are assigned which depend critically on the anisotropy.

The experimental evidence is that He–C_2H_2 lies close to the free-rotor limit. This is consistent with IPESA, which is less anisotropic than IPESB as indicated by Fig. 5. We conclude that RWPS is not yet accurate enough to discriminate between different high quality theoretical structures for this complex and that IPESA currently provides a superior overall fit to the experimental data and better reflects the actual anisotropy of the complex.

VII. DISCUSSION AND CONCLUSIONS

A. Comparison of Coriolis model parameters

The differences between the v = 0 and 1 experimental parameters in Table II are mostly not large, but they are still sufficient to give the $j = 1 \leftarrow 0$ and $0 \leftarrow 1$ subbands rather different appearances (Figs. 2 and 3). In our previous work,[5] which was limited to $j = 1 \leftarrow 0$, we only had theoretical $j = 1$ Coriolis parameters for v = 0 and experimental ones for v = 1. Now that parameters for v = 0, $j = 1$ can be directly compared (Table II), we find that experiment is closer to theory in one important respect, namely, the π − σ splitting, $E_v(1\pi) - E_v(1\sigma)$ (previously called 2α). This quantity has experimental values of 0.502 and 0.429 cm^{-1} for v = 0 and 1, respectively, as compared to a theoretical value of 0.674 cm^{-1}.

So theory (based on IPESA) is significantly closer to the new v = 0 value, though still too large in magnitude (further from the free rotor limit). On the other hand, the theoretical B-values and β-value (Coriolis interaction) are slightly closer to their experimental v = 1 counterparts.

Interpretation of the $j = 2$ parameters is more difficult, and in any case we necessarily compare theory for v = 0 with experiment for v = 1. But there is at least reasonable accord. The σ, π, and δ states have the same energy ordering and roughly similar energy spacing, with the experimental levels tending to be slightly lower in energy. The B-values are fairly similar to each other and to those for $j = 1$, but their ordering is opposite in experiment and theory. Both experiment and theory have a Coriolis parameter $\gamma(2)$ (linking π and δ levels) which is a bit smaller than $\beta(2)$ (linking σ and π levels).

B. Free rotor quantum number *L*

So far, we have labelled rotational levels using quantum numbers J, j, p (=e or f), and K (=σ, π, δ, that is, 0, 1, 2) which are interpreted as the projection of J on the intermolecular axis. There is an alternate free-rotor labelling scheme, namely, J, j, L, where L represents the end-over-end rotation of He relative to C_2D_2, and J is the vector sum of j and L. For completeness, we include the appropriate L labels in the Tables. Note (Table I) that levels with equal j and L values indeed tend to have similar energies even though they differ in J. The quantity $(J + j + L)$ is even for levels with e parity, and odd for f parity.

Since the He–C_2D_2 infrared dipole transition moment is attached to C_2D_2, the selection rule for fully allowed transitions is $\Delta L = 0$. In addition, of course, we have $\Delta j = \pm 1$, and $\Delta J = 0, \pm 1$. In Tables III and IV, we see that the $\Delta L = 0$ rule is indeed followed except for a few $\Delta L = 2$ transitions which are weak and located far from their band center. These "forbidden" transitions remind us that L (like j and K) is not a rigorously good quantum number.

C. Comparison with He–CO

It is interesting to compare energy levels of He–C_2D_2 with those of He–CO,[33–35] as shown in Fig. 6. Acetylene and carbon monoxide are isoelectronic, which suggests similar intermolecular potential energy surfaces. Moreover, the reduced mass is the same for the pairs He–$^{12}C_2D_2$ and He–$^{12}C^{16}O$, so the dimer B-values should also be alike (in fact, $B \approx 0.29$ cm^{-1} for He–CO and 0.24 cm^{-1} for He–C_2D_2). Similarities are indeed evident in Fig. 6, but, of course, there are important differences as well. The CO monomer B-value is more than twice that of C_2D_2 (1.92 vs. 0.85 cm^{-1}), so the $j = 1$ levels of He–CO lie much higher and the $j = 2$ levels are not even bound. He–CO is basically T-shaped, while He–C_2D_2 is linear, so 1σ lies above 1π for He–CO (see Fig. 6). CO lacks the symmetry of C_2D_2 ($D_{\infty h}$), which means that weak infrared transitions with $\Delta j = 0$ can be observed for He–CO, and that even- and odd-j levels within a given vibrational state can interact.

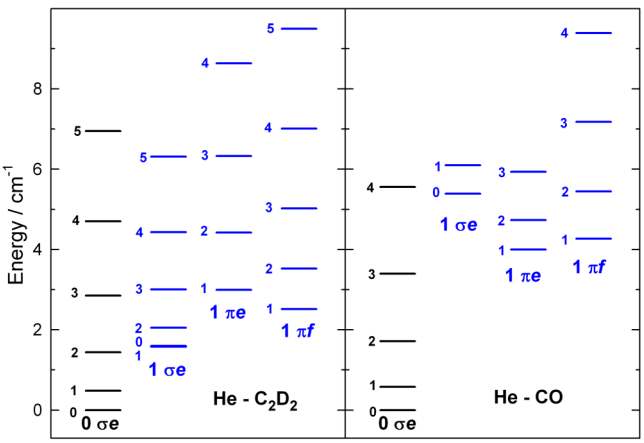

FIG. 6. Comparison of experimentally determined energy level patterns for He–C_2D_2 (Table I) and He – CO.[35] Levels with $j = 2$ are not shown for He–C_2D_2 (cf. Fig. 1) and are not bound for He–CO.

D. Microwave prediction and conclusions

No pure rotational microwave spectra have yet been reported for helium–acetylene. Such transitions arise from an induced dipole moment and will thus be very weak, but their detection should still be feasible as shown by the case of neon–acetylene.[7] Such microwave spectra would be much more precise and accurate than the infrared and RWPS spectra discussed here. Our "experimental" energy levels in Table II predict three possible low temperature He–C_2D_2 transitions in the 14 GHz region: $0\sigma R(0) \approx 14.52$; $1\sigma R(1) \approx 14.56$; and $1\pi\ Q(1) \approx 13.46$ GHz.

In conclusion, we have extended the analysis of the infrared spectrum of He–C_2D_2 to include transitions corresponding to $P(1)$ and $R(1)$ of the monomer, in addition to the previously studied $R(0)$ region. The analysis was guided by energy level calculations based on the *ab initio* CCSD(T) intermolecular potential of Fernández *et al.*,[22] and there is reasonably good agreement between theoretical and experimental levels. Further guidance came from the Coriolis model,[26,27] applied here to $j = 2$ levels, which gave fairly good energies as well as extremely useful intensity predictions. The present results provide a stringent test for current and future quantum chemical calculations on this rather fundamental helium–acetylene system. Indeed we have argued that these spectra allow one to discriminate between the two best and most recent extant potential energy surfaces, IPESA and IPESB.

ACKNOWLEDGMENTS

We gratefully acknowledge the financial support of the Natural Sciences and Engineering Research Council of Canada and the Canadian Space Agency. This work has been supported by the Ministerio de Ciencia e Innovación (CTQ2011-29311-C02-01 project), and by the U.S. National Science Foundation through Grant No. CHE-1300504.

[1]L. J. Danielson, K. M. McLeod, and M. Keil, J. Chem. Phys. **87**, 239 (1987).
[2]L. J. Danielson, M. Keil, and P. J. Dunlop, J. Chem. Phys. **88**, 4218 (1988).
[3]T. Slee, R. J. L. Roy, and C. E. Chuaqui, Mol. Phys. **77**, 111 (1992).
[4]R. Moszynski, P. E. S. Wormer, and A. van der Avoird, J. Chem. Phys. **102**, 8385 (1995).
[5]M. Rezaei, N. Moazzen-Ahmadi, A. R. W. McKellar, B. Fernandez, and D. Farrelly, Mol. Phys. **110**, 2743 (2012).

[6]R. J. Bemish, L. Oudjeans, R. E. Miller, R. Moszynski, T. G. A. Heijman, T. Korona, P. E. S. Wormer, and A. van der Avoird, J. Chem. Phys. **109**, 8968 (1998).
[7]Y. Liu and W. Jäger, Phys. Chem. Chem. Phys. **5**, 1744 (2003).
[8]R. L. DeLeon and J. S. Muenter, J. Chem. Phys. **72**, 6020 (1980).
[9]Y. Ohshima, M. Iida, and Y. Endo, Chem. Phys. Lett. **161**, 202 (1989).
[10]T. A. Hu, D. G. Prichard, L. H. Sun, J. S. Muenter, and B. J. Howard, J. Mol. Spectrosc. **153**, 486 (1992).
[11]Y. Ohshima, Y. Matsumoto, M. Takami, and K. Kuchitsu, J. Chem. Phys. **99**, 8385 (1993).
[12]R. J. Bemish, P. A. Block, L. G. Pedersen, W. T. Yang, and R. E. Miller, J. Chem. Phys. **99**, 8585 (1993).
[13]R. J. Bemish and R. E. Miller, Chem. Phys. Lett. **281**, 272 (1997).
[14]Y. Liu and W. Jäger, J. Mol. Spectrosc. **205**, 177 (2001).
[15]P. Macko, C. Lauzin, and M. Herman, Chem. Phys. Lett. **445**, 113 (2007).
[16]C. Lauzin, K. Didriche, P. Macko, J. Demaison, J. Lievin, and M. Herman, J. Phys. Chem. A **113**, 2359 (2009).
[17]C. Lauzin, L. H. Coudert, M. Herman, and J. Lievin, J. Phys. Chem. A **117**, 13767 (2013).
[18]C. Lauzin and K. Didriche, Phys. Chem. Chem. Phys. **13**, 751 (2011).
[19]C. Lauzin, E. Cauet, J. Demaison, M. Herman, H. Stoll, and J. Lievin, Mol. Phys. **110**, 2751 (2012).
[20]G. Galinis, L. G. M. Luna, M. J. Watkins, A. M. Ellis, R. S. Minns, M. Mladenović, M. Lewerenz, R. T. Chapman, I. C. E. Turcu, C. Cacho, E. Springate, L. Kazak, S. Göde, R. Irsig, S. Skruszewicz, J. Tiggesbäumker, K.-H. Meiwes-Broer, A. Rouzée, J. G. Underwood, M. Sianoi, and K. von Haeften, Faraday Discuss. **171**, 195 (2014).
[21]G. Galinis, C. Cacho, R. T. Chapman, A. M. Ellis, M. Lewerenz, L. G. M. Luna, R. S. Minns, M. Mladenović, A. Rouzée, E. Springate, I. D. E. Turcu, M. J. Watkins, and K. von Haeften, Phys. Rev. Lett. **113**, 043004 (2014).
[22]B. Fernández, C. Henriksen, and D. Farrelly, Mol. Phys. **111**, 1173 (2013).
[23]P. F. Bernath, *Spectra of Atoms and Molecules* (Oxford University Press, New York, 1995), pp. 328-329.
[24]C. R. Munteanu and B. Fernández, J. Chem. Phys. **123**, 014309 (2005).
[25]J. M. Hutson, BOUND, version 5: A program for calculating bound-state energies for weakly bound molecular complexes distributed via Collaborative Computing Project No. 6 of the Science and Engineering Research Council on Molecular Quantum Dynamics, UK Technical Report, 1993.
[26]M. D. Brookes, D. J. Hughes, and B. J. Howard, J. Chem. Phys. **104**, 5391 (1996).
[27]M. Wangler, D. A. Roth, G. Winnewisser, I. Pak, and A. R. W. McKellar, Can. J. Phys. **79**, 423 (2001).
[28]N. Moazzen-Ahmadi and A. R. W. McKellar, Int. Rev. Phys. Chem. **32**, 611 (2013).
[29]C. Lauzin, N. Moazzen-Ahmadi, and A. R. W. McKellar, J. Mol. Spectrosc. **269**, 124 (2011).
[30]J. Norooz Oliaee, N. Moazzen-Ahmadi, and A. R. W. McKellar, Mol. Phys. **110**, 2797 (2012).
[31]A. G. Maki and J. S. Wells, *Wavenumber Calibration Tables from Heterodyne Frequency Measurements* (National Institute of Standards and Technology, Washington, DC, 1991), http://physics.nist.gov/PhysRefData/wavenum/html/contents.html.
[32]C. M. Western, PGOPHER version 8.0, University of Bristol Research Data Repository, 2014.
[33]C. Chuaqui, R. J. L. Roy, and A. R. W. McKellar, J. Chem. Phys. **101**, 39 (1994).
[34]M.-C. Chan and A. R. W. McKellar, J. Chem. Phys. **105**, 7910 (1996).
[35]A. R. W. McKellar, Y. Xu, W. Jäger, and C. Bissonnette, J. Chem. Phys. **110**, 10766 (1999).
[36]S. Ghersetti and K. Narahari Rao, J. Mol. Spectrosc. **28**, 27 (1968).